LANGLEY
GRANT
IN-34-CR
204463
P16.

FINAL TECHNICAL REPORT

on

NAG-1-866

COMPUTATIONAL FLUID DYNAMICS RESEARCH IN THREE-DIMENSIONAL ZONAL TECHNIQUES

Robert W. Walters - Principal Investigator
Department of Aerospace and Ocean Engineering
Virginia Polytechnic Institute and State University

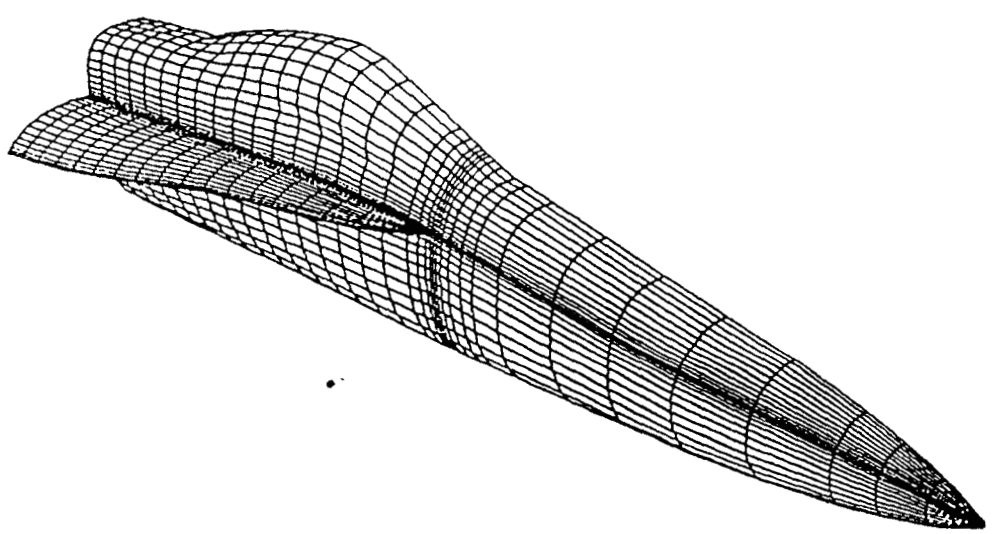

April 1989

SUMMARY

Patched-grid algorithms for the analysis of complex configurations with an implicit, upwind-biased Navier-Stokes solver have been investigated. Conservative and non-conservative approaches for performing zonal interpolations were implemented. The latter approach yields the most flexible technique in that it can handle both patched and overlaid grids. Results for a two-dimensional blunt body problem show that either approach yield accurate steady-state shock locations and jump conditions. In addition, calculations of the turbulent flow through a hypersonic inlet on a three-zone grid show that the numerical prediction is in good agreement with the experimental results[1]

Through the use of a generalized coordinate transformation at the zonal interface between two or more blocks, the algorithm can be applied to highly stretched viscous grids and to arbitrarily-shaped zonal boundaries. Applications were made to the F-18 aircraft at subsonic, high-alpha conditions, in support of the NASA High-Alpha Research Program. The calculations were compared to ground-based and flight test experiments and have been used as a guide to understanding the ground-based tests, which are laminar and transitional, and their relationship to flight[2,3]. Calculations about a complete reconnaissance aircraft were also performed in order to further demonstrate the capability of the patched-grid algorithm[4].

During the period of this grant, the papers in the references section were written which cover in detail the three-dimensional zonal techniques that were investigated in this study. As such, they have been included as the body of this final report.

REFERENCES

1. Thomas, J.L., Rudy, D.H., Chakravarthy, S.R., and Walters, R.W. 'Patched-Grid Computations of High-Speed Inlet Flows', Symposium on Advances and Applications in Computational Fluid Dynamics, Chicago, Illinois, ASME FED Vol. 66, pp. 193-199.
2. Thomas, J.L., Walters, R.W., Reu, T., Ghaffari, F., Weston, R.P., and Luckring, J.M., 'A Patched-Grid Algorithm for Complex Configurations Directed Towards the F-18 Aircraft', AIAA Paper No. 89-0121, 1989.
3. Thomas, J.L. and Walters, R.W., *Navier-Stokes Computations for Aerodynamic Configurations at High Angles of Attack*, to appear, 1990.
4. Walters, R.W. and Thomas, J.L. 'A Patched-Grid Algorithm for Complex Aircraft Configurations', SIAM Conference on Domain Decomposition Methods, March, 1989.

PATCHED-GRID COMPUTATIONS OF HIGH-SPEED INLET FLOWS

James L. Thomas
David H. Rudy
NASA Langley Research Center
Hampton, Virginia 23665

Sukumar R. Chakravarthy
Rockwell International Science Center
Thousand Oaks, California 91360

R. W. Walters
Virginia Polytechnic Institute and State University
Blacksburg, Virginia 24061

Symposium on Advances and Applications
in Computational Fluid Dynamics
Winter Annual Meeting of ASME
Chicago, Illinois
November 28-December 2, 1988

PATCHED-GRID COMPUTATIONS OF HIGH-SPEED INLET FLOWS

James L. Thomas
David H. Rudy
NASA Langley Research Center
Hampton, Virginia 23665

Sukumar R. Chakravarthy
Rockwell International Science Center
Thousand Oaks, California 91360

R. W. Walters
Virginia Polytechnic Institute and State University
Blacksburg, Virginia 24061

ABSTRACT

Implicit algorithms for the compressible Navier-Stokes equations are applied to the computation of high-speed inlet flows typical of those encountered on propulsion systems of advanced hypersonic vehicles. Patched grids are used to accurately treat blunt cowl shock-shock interaction effects at the inlet entrance and efficiently compute effects due to variations in the downstream inlet geometry. Two algorithms, each incorporating upwind-biased spatial differencing for the convective and pressure terms within a flux-difference-splitting framework, are compared to experimental data for internal compression ratios of two and eight at a nominal Mach number of 7.4. Results from the two codes, each with an algebraic turbulence model, agree closely with each other and predict the overall boundary layers of velocity and temperature reasonably well, although a definitive assessment is not possible because of uncertainties in the experimental data accuracy.

NOMENCLATURE

A	Jacobian matrix
F, G	inviscid fluxes
F_v, G_v	viscous fluxes
J	transformation Jacobian
L	reference length, also difference operator
M	Mach number
Pr	Prandtl number, taken as 0.72
Q	conservation variables
Re_L	Reynolds number, $Re_L = \tilde{\rho}_\infty \tilde{u}_\infty \tilde{L}/\tilde{\mu}_\infty$
T	temperature, also diagonalizing matrices
U, V	contravariant velocities
a	speed of sound
e	total energy per unit volume
p	static pressure, $p = (\gamma - 1)[e - \rho(u^2 + v^2)/2]$
p_p	pitot pressure
q	vector for state interpolations
$\dot{q}_{x_i}$	heat flux terms
t	time
u, v	Cartesian velocities in x and y directions
x, y	Cartesian coordinates
Δt	time step
ΔQ	change in Q over time step Δt
γ	ratio of specific heats, taken as 1.4
ξ, η	general curvilinear coordinates
κ	spatial differencing parameter
λ	coefficient of bulk viscosity, $\lambda + 2\mu/3 = 0$
Λ	diagonal matrix of eigenvalues
μ	coefficient of molecular viscosity
ρ	density
$\tau_{x_i x_j}$	viscous shear stress terms

Subscripts:

x,y	denotes differentiation with respect to x,y
t	denotes total conditions
w	denotes wall value
∞	denotes conditions at freestream

Superscripts:

^	denotes quantities in generalized coordinates
~	denotes dimensional value or Roe-averaging

INTRODUCTION

There is an increasing effort in the development and validation of computational methods for high-speed flows because of the renewed interest in the hypersonic flight regime such as, for example, in the National Aero-Space Plane project. The propulsion system of advanced hypersonic vehicles will likely use the external vehicle contours as compression and expansion surfaces for the inlet and nozzle, respectively, and thus the engine-airframe integration is a critical consideration. The proper prediction of mass flow into the inlet is dependent on the accuracy to which the developing boundary layers on the forebody compression surfaces can be predicted. High heating rates will occur on the blunt cowl lip at the inlet entrance and vary considerably with Mach number and incidence because of the shock-shock interactions. The design of such systems relies heavily on the development of computational fluid dynamic codes with the required geometric flexibility and requisite physical models, since many of the high-enthalpy, high Mach number conditions cannot be simulated with ground-based facilities.

Two recently-developed algorithms for the compressible Navier-Stokes equations are applied to two high-speed inlets which have features representative of those encountered in the propulsion systems of advanced hypersonic inlets. The inlets were tested experimentally in the 3.5 Foot Hypersonic Tunnel at NASA Ames Research Center (Gnos et al., 1973) at a nominal freestream Mach number of 7.4 and Reynolds number of 8.86 x 10^6 per meter. The inlets tested were identical on the compression surfaces ahead of the inlet and the internal inlet geometry was varied to provide internal compression ratios of two, eight, and twelve, leading to the designations P2, P8, and P12 inlets, respectively. Only the P2 and P8 inlets are studied here since the P12 inlet had fluctuations in surface pressures which prevented detailed experimental measurements.

The present work is a follow-on to a previous study (Rudy et al., 1988) in which results from central and upwind difference codes were compared for the P8 inlet with a tangent wedge geometric approximation to the blunt cowl lip. A patched grid formulation is used here to accurately treat the blunt cowl interaction with the forebody compression field and efficiently treat variations in inlet geometry downstream of the inlet entrance. Results from the two implicit finite-volume algorithms, each based on an upwind-biased spatial differencing approach for the convective and pressure terms within a flux-difference-splitting framework, are compared with experimental results for both inlets. The turbulence is modeled here with an algebraic eddy-viscosity model (Baldwin and Lomax, 1978), although alternate models could easily be investigated, such as in the related recent work of Ng et al. (1988).

SEMI-DISCRETE FORMULATION

The two algorithms used are both implicit finite-volume algorithms. The first, CFL3D (Computational Fluids Lab 3-D code), was developed by Thomas et al. (1985,1987) for the thin-layer Navier-Stokes equations. The second, USA-PG2 (Unified Solution Algorithm - Perfect Gas, 2-D code), was developed by Chakravarthy et al. (1985,1988). Both codes solve the time-dependent two-dimensional compressible Navier-Stokes equations expressed in strong conservation law form and generalized coordinates as below.

$$\frac{\partial \widehat{Q}}{\partial t} + \frac{\partial(\widehat{F} - \widehat{F}_v)}{\partial \xi} + \frac{\partial(\widehat{G} - \widehat{G}_v)}{\partial \eta} = 0 \qquad (1)$$

$$\widehat{Q} = \frac{Q}{J} = \frac{1}{J}\begin{bmatrix} \rho \\ \rho u \\ \rho v \\ e \end{bmatrix}$$

$$\widehat{F} = \frac{1}{J}\begin{bmatrix} \rho U \\ \rho U u + \xi_x p \\ \rho U v + \xi_y p \\ (e+p)U \end{bmatrix} \qquad \widehat{F}_v = \frac{1}{J}\begin{bmatrix} 0 \\ \xi_x \tau_{xx} + \xi_y \tau_{xy} \\ \xi_x \tau_{yx} + \xi_y \tau_{yy} \\ \xi_x b_x + \xi_y b_y \end{bmatrix}$$

$$\widehat{G} = \frac{1}{J}\begin{bmatrix} \rho V \\ \rho V u + \eta_x p \\ \rho V v + \eta_y p \\ (e+p)V \end{bmatrix} \qquad \widehat{G}_v = \frac{1}{J}\begin{bmatrix} 0 \\ \eta_x \tau_{xx} + \eta_y \tau_{xy} \\ \eta_x \tau_{yx} + \eta_y \tau_{yy} \\ \eta_x b_x + \eta_y b_y \end{bmatrix}$$

$$U = \xi_x u + \xi_y v \qquad V = \eta_x u + \eta_y v$$

The variables ξ and η correspond to the coordinates parallel and normal to the inlet walls, respectively. The equations are nondimensionalized by $\tilde{\rho}_\infty$, $\tilde{a}_\infty$, $\tilde{\mu}_\infty$, and $\tilde{L}$. The shear stress and heat flux terms are defined in tensor notation for laminar flow as:

$$\tau_{x_i x_j} = \frac{M_\infty}{Re_L}\left[\mu(\frac{\partial u_i}{\partial x_j} + \frac{\partial u_j}{\partial x_i}) + \lambda \frac{\partial u_k}{\partial x_k}\delta_{ij}\right]$$

$$\dot{q}_{x_i} = -\left[\frac{M_\infty \mu}{Re_L Pr(\gamma - 1)}\right]\frac{\partial (a^2)}{\partial x_i}$$

where $b_{x_i} = u_j \tau_{x_i x_j} - \dot{q}_{x_i}$ and Sutherland's law is used for the variation of molecular viscosity with temperature.

The equations are represented with a semi-discrete finite-volume formulation. Integrating (1) over a cell volume bounded by surfaces of constant ξ and η gives

$$\begin{aligned}(\frac{\partial \widehat{Q}}{\partial t})_{i,j} &= -\widehat{R}_{i,j} \\ &= -(\widehat{F} - \widehat{F}_v)_{i+1/2,j} + (\widehat{F} - \widehat{F}_v)_{i-1/2,j} \\ &\quad -(\widehat{G} - \widehat{G}_v)_{i,j+1/2} + (\widehat{G} - \widehat{G}_v)_{i,j-1/2}\end{aligned} \tag{2}$$

where the subscripts i,j denote evaluation at cell-centered locations corresponding to ξ_i, η_j, respectively. A uniform spacing is taken in the computational domain, i.e. $\xi_{i+1,j} - \xi_{i,j} = 1$, such that the cell volume is associated with the discrete evaluation of the inverse of the transformation Jacobian.

The term $\widehat{R}$ represents the steady-state residual, the accuracy of which is determined by the spatial differencing, discussed subsequently. The equations are advanced implicitly in time to a steady state with a spatially-factored algorithm in delta form

$$L_\xi L_\eta \Delta \widehat{Q} = -\Delta t \, \widehat{R} \tag{3}$$

For efficiency, first-order spatial differencing is used on the left-hand side operators and an approximate diagonal inversion is used in the ξ direction, along which the grid is not highly stretched.

SPATIAL DIFFERENCING

The spatial differencing for the convective and pressure terms uses a MUSCL (Monotone Upstream-Centered Conservation Law) approach to evaluate the interface flux. The interface flux in the ξ direction, for example, is constructed along a line of constant η_j as

$$\begin{aligned}\widehat{F}_{i+1/2} &= \widehat{F}(q^-, q^+)_{i+1/2} \\ &= \widehat{F}(\, q_{i-1}\,,\, q_i\,,\, q_{i+1}\,,\, q_{i+2}\,,\, (\nabla\xi/J)_{i+1/2})\end{aligned} \tag{4}$$

where $q^{\pm}_{i+1/2}$ denote state variables determined from upwind-biased interpolations to the left and right of the i+1/2 cell interface location as

$$\begin{aligned}(q^-)_{i+1/2} &= q_i + \{\frac{1}{4}[(1-\kappa)\overline{\Delta}_- + (1+\kappa)\overline{\Delta}_+]\}_i \\ (q^+)_{i+1/2} &= q_{i+1} - \{\frac{1}{4}[(1-\kappa)\overline{\Delta}_+ + (1+\kappa)\overline{\Delta}_-]\}_{i+1}\end{aligned} \tag{5}$$

where

$$(\Delta_+)_i = q_{i+1} - q_i \qquad (\Delta_-)_i = q_i - q_{i-1}$$

The parameter κ determines the order of the scheme in smooth regions ($\kappa = 1/3$ corresponds to the third-order formulation and is used herein) and slope limiting is used to maintain monotonicity across discontinuities in the flow, such as shock waves,

$$\begin{aligned}\overline{\Delta}_+ &= \max[0, \min(\Delta_+ \mathrm{sgn}\Delta_-, \beta\Delta_- \mathrm{sgn}\Delta_+)]\mathrm{sgn}\Delta_+ \\ \overline{\Delta}_- &= \max[0, \min(\Delta_- \mathrm{sgn}\Delta_+, \beta\Delta_+ \mathrm{sgn}\Delta_-)]\mathrm{sgn}\Delta_-\end{aligned} \tag{6}$$

where $\beta = (3-\kappa)/(1-\kappa)$. The state-variable interpolations are done on the vector q, which in the case of CFL3D is taken as the primitive variables, $q = (\rho, u, v, p)^T$. In the case of USA-PG2, the characteristic variables are used, $q = \widehat{T}^{-1}Q$, where $\widehat{T}^{-1}$ corresponds to the matrix of left eigenvectors of the Jacobian matrix, $\widehat{A} = \partial\widehat{F}/\partial\widehat{Q}$.

The flux is constructed through the solution of a local Riemann problem at the interface using the flux-difference-splitting approach of Roe (1981), which can be written in terms of the conserved variables at the interface as

$$F_{i+1/2} = \frac{1}{2}\left[\, \widehat{F}(Q^+) + \widehat{F}(Q^-) - |\tilde{A}|\,(Q^+ - Q^-)\,\right]_{i+1/2} \tag{7}$$

where $|\tilde{A}| = \tilde{T}\,|\tilde{\Lambda}|\,\tilde{T}^{-1}$ is evaluated with Roe-averaged variables such that $\widehat{F}^+ - \widehat{F}^- = \tilde{A}(Q^+ - Q^-)$. The algebraic form of the equations simplifies to a considerable degree when the primitive or characteristic variables are used for the state-variable interpolations, and all choices recover identical results for first-order spatial differencing. The scheme has the property of capturing strong shocks sharply and providing minimal dissipation levels in wall-bounded viscous flows (Van Leer, 1987).

The shear stress and heat transfer terms are centrally differenced, corresponding to a second-order spatial discretization. The code CFL3D solves the thin-layer form of the equations while USA-PG2 solves the complete equations. Both formula-

tions model the turbulence using the two-layer eddy-viscosity model of Baldwin and Lomax (1978).

PATCHED GRID ALGORITHM

Zonal and/or patched grids are attractive because they can substantially reduce the difficulties associated with the generation of grids over complex geometries. Additionally, they generally lead to a more efficient algorithm by tailoring the grids to the local geometry, thereby eliminating inefficient grid topologies, and by using mathematical models in each zone appropriate to the local physics. The two requirements placed upon a patched grid algorithm are accuracy and conservation. Rai (1985) demonstrated these two requirements could be met by conservatively interpolating the flux across a zonal boundary, so as to preserve the spatial flux of mass, momentum, and energy.

An alternate approach is taken here. Across a zonal interface, conserved variables are conservatively interpolated from zone 2, for example, onto the grid locations corresponding to an analytic continuation of the grid points in zone 1. These interpolated points are used to construct the interface flux at the zone 1 boundary through the solution of an underlying Riemann problem. The interpolated variables are conservatively constructed, much as the spatial fluxes are interpolated in the spatially conservative approach, such that they reflect the correct amount of mass, momentum, and energy contained in zone 2. Likewise, zone 1 data is conservatively interpolated onto an analytic continuation of the grid points in zone 2 in order to construct the interface flux at the zone 2 boundary. The algorithm is constructed so that if a geometric match between the grid points exists at the zonal interface, the scheme recovers identically the interior scheme discussed previously. Thus, there can be a slight mismatch in the spatial flux across a zonal boundary, on the order of the local truncation error of the scheme. The advantage of this approach is that it can readily be extended to more general situations, such as overlapped grids where the zonal boundaries need not be coincident.

The effectiveness of the approach in maintaining conservation and accuracy across the interface is demonstrated for a supersonic blunt body calculation similar to that used previously by Rai (1985). A single grid and a three-zone grid are shown in fig. 1. Pressure contours for a freestream Mach number of 2 are shown in fig. 2 and show remarkable correspondence between the computed shock locations for both cases; for the 3-zone grid, a zone boundary crosses the shock position near the plane of symmetry and near the downstream boundary of the grid.

Figure 3 shows pressure contours for two different zonal boundary locations, one upstream of the shock location and one downstream. Other than a thickening of the shock pressure contours in the regions of coarser grid zones, the zonal grids show very little sensitivity to the zonal boundary.

INLET DESCRIPTION

The zonal topology used for the inlet computations is shown in fig. 4 for both the P8 and P2 inlets. Zones 1, 2, and 4 are H-type grids clustered in the region near the wall, containing 101 x 101, 12 x 51, and 151 x 101 grid points, respectively. The normal spacing at the wall at the inlet entrance station, x = 32 in. (81.28 cm), is .0002 in. (.005 cm), resulting in turbulent inner-layer similarity parameter values on the order of unity along the walls. Zone 3 is a C-type grid describing the local geometry of the blunt cowl lip at the inlet entrance station, spanning from x = 31 in. to x=32 in., and containing 201 x 101 grid points. An enlarged view of the grid near the inlet entrance is shown in fig. 5, where for clarity a subset of the complete grid in zone 3 is shown.

The P2 and P8 inlets represent inlet configurations typical of a hypersonic airbreathing vehicle. The 2-D inlets were designed to provide an internal compression ratio of 2 and 8, respectively. The forebody wedge is a 6.5 deg. wedge intended to match a design Mach number of 6 at the inlet entrance under the test conditions of a freestream Mach number of 7.4, allowing for boundary-layer displacement effects. The centerbody geometries for the two inlets are identical upstream of x = 44.25 in. (112.39 cm) and the cowl geometries are identical upstream of x = 34.25 in. (87 cm). Since the inlet entrance flow is predominantly an attached supersonic flow, the zonal topology lends itself to an efficient solution procedure. For example, the solution in zone 1 can be obtained first. Then the solutions in zones 2-3 can be obtained simultaneously. These zones then serve as initial value solutions for the solution in zone 4 for either inlet. In addition, the solution for the P2 inlet was obtained by restarting from the P8 flowfield. Although Navier-Stokes solutions are obtained here, a further savings could be effected by substituting parabolized approximations for the attached weak-interaction regions in zones 1, 2, and 4.

The Reynolds number based on freestream conditions is 8.86 x 10^6 per meter. The total pressure is

4.14 x 10^6 N/m^2, the total temperature is 811 deg. K, and the wall temperature is 303 deg. K. In the experiment, transition to turbulence occurred on both the centerbody and the cowl surfaces for the P8 inlet. Transition regions were specified to correspond approximately to the experimental values. The turbulent eddy viscosity was linearly increased from zero to the fully-turbulent value over a length of 5.9 in. (15 cm) along the centerbody beginning at 10.8 in. (27.5 cm) and over a length of 3.94 in. (10 cm) along the cowl surface beginning at 39.8 in. (101 cm). Although not shown, the transitional computations and the experiment both indicate a boundary-layer thickness of about 0.5 in. at the inlet entrance station. These same transitional locations were used for the P2 inlet, although analysis of the velocity profiles in the inlet (Gnos et al., 1973) indicates that the boundary layers remain laminar on the cowl surface. All of the calculations were made with a γ of 1.4, corresponding to equilibrium conditions at the tunnel test section.

P8 INLET RESULTS

Mach number contours in the region of the blunt cowl lip at the inlet entrance station are shown in fig. 6 and pressure contours at the blunt cowl lip are shown in fig. 7. The forebody wedge shock passes smoothly through the zonal interface between zones 1 and 3. Because the grid in zone 3 is much finer than that in zone 1, the pressure contours coalesce slightly downstream of the zonal interface, owing to a finer resolution of the shock. The inlet forebody shock is much weaker than the detached shock that develops on the blunt cowl lip and there is consequently only a minor interaction on the upper surface of the cowl. The detached shock on the underside of the cowl passes smoothly across the interface between zones 3 and 4, as do the Mach contours associated with the boundary layer development on the cowl. Although not shown, the results agree closely with Schlieren photographs from the experiment.

Computed and measured pressures along the inlet cowl and centerbody are shown in fig. 8; density and pressure contours of the inlet flowfield are shown in fig. 9. The computed pressures agree closely with the experiment over the centerbody, including the pressure rise associated with the impingement of the cowl shock onto the centerbody at x=44 in. The computed pressures on the cowl are higher than those measured in the region before the impingement of the reflected shock from the centerbody onto the cowl surface at x=49 in. The reflected shock impingement is predicted slightly downstream of that measured, although the overall pressure rise through the interaction is well predicted. From previous work, it is known that the impingement location is very sensitive to the boundary layer development on the centerbody.

Predicted pitot-pressure and total-temperature profiles are compared in fig. 10 with experimental data. In fig. 10(a), both codes predict a pitot pressure ratio of .025 in the inviscid core region above the boundary layer and below the cowl shock. This value is higher than the experimental value of .021. Ng, Benson, and Kunik (1986) demonstrated close agreement with the experimentally-measured level in that region using a γ of 1.38. However, this choice of γ cannot be justified based on the temperature present in the experiment, as the freestream value of temperature is no more than approximately 100 deg. K. Thus, the ratio of specific heats would be expected to be 1.4 in the inviscid portions of the flow. Real-gas effects may be important, however, in the flow field induced by the presence of the pitot probe since the temperature increases rapidly across the shock ahead of the tube to a value near that of reservoir conditions. Pitot-tube pressures were calculated with equilibrium real-gas relations, but only a slight effect was found; the effect of the equilibrium real-gas assumption becomes more important at higher stagnation temperatures. Additional supporting evidence is provided by the equilibrium air calculations by Ota et al. (1988) which indicate constant specific heats throughout the inlet.

The Mach number at the cowl inlet station outside of the wedge shock determined from real-gas pitot formulas using the measured pitot pressure data is 7.6. This indicates a longitudinal variation in Mach number of approximately 0.01 per foot, which is in agreement with the wind-tunnel calibration measurements (Appendix A of Gnos et al. (1973)). Agreement of the computed and experimental pitot pressures may require incorporation of the longitudinal Mach-number gradient into the calculations. In addition, the measured total temperatures do not recover to the freestream total temperature in the inviscid core regions of the inlet.

With these discrepancies in mind, examination of the profiles indicates generally good agreement of the boundary layer thicknesses of temperature and pitot pressure on both the centerbody and the cowl. The location of the cowl shock at x=41 in. is predicted in better agreement with the experiment than the previous result (Rudy et al., 1988) which used a tangent wedge approximation for the cowl. The two compu-

tations agree closely with each other and predict the overall trends in pitot pressure and temperature at x=44 in., corresponding to the cowl shock impingement on the centerbody, and at x=47 in., just downstream of the cowl shock impingement. The pitot profiles at x=49.5 in. reflect the fact that the computed impingement of the reflected shock from the centerbody onto the cowl is predicted downstream of the experiment, to a somewhat lesser extent with the computations from USA-PG2 than with CFL3D.

P2 INLET RESULTS

Comparisons of the computed and experimental results for the P2 inlet are shown in figs. 11-13. The centerbody pressure comparisons indicate that the location of the pressure increase at x=44.5 in. associated with the cowl shock impingement is predicted accurately but the overall pressure rise is substantially higher than the experiment. The cowl pressures show little variation because the reflected shock from the centerbody passes downstream beneath the cowl surface, as can be seen from the flowfield contours in fig. 12, which are in good agreement with Schlieren photographs from the experiment. Also, the cowl shock position evident in the profiles at x=40 in. and x=43 in. is well predicted.

As for the P8 inlet, given the discrepancies in measured pitot pressures and total temperatures, the boundary layer thicknesses are generally predicted accurately. The decrease in the boundary layer thickness downstream of the cowl shock impingement is well predicted. The predicted boundary layer thickness on the cowl is slightly greater than the experimental results, associated with the observation that the experimental boundary layer remained laminar on the cowl surface. Calculations made with a laminar model on the cowl predicted a slightly thinner boundary layer, with a resultant improvement in the comparisons.

CONCLUDING REMARKS

Two implicit algorithms for the compressible Navier-Stokes equations have been applied to the computation of high-speed inlet flows typical of those which will be encountered on propulsion systems of advanced hypersonic vehicles. Patched grids have been used to accurately treat blunt cowl shock-shock interaction effects at the inlet entrance and efficiently compute effects due to variations in the downstream inlet geometry. The algorithms considered are similar, each incorporating upwind-biased spatial differencing for the convective and pressure terms within a flux-difference-splitting framework. The results from the two codes agree closely, lending confidence that the equations and turbulence model are being solved correctly with sufficient resolution, which is a necessary step in the code validation process. The comparisons with experimental data for internal compression ratios of two and eight at a nominal Mach number of 7.4 indicate that the overall features of the inlet flowfield are predicted reasonably well, including the boundary layer thicknesses of velocity and temperature. However, because of uncertainties in the experimental data accuracy, a definitive assessment of the accuracy of the turbulence model is not possible.

REFERENCES

Baldwin, B. S. and Lomax, H., 1978, "Thin-Layer Approximation and Algebraic Models for Separated Turbulent Flows," AIAA 78-257.

Chakravarthy, S. R., Szema, K-Y., Goldberg, U. C., Gorski, J. J. and Osher, S., 1985, "Application of a New Class of High Accuracy TVD Schemes to the Navier-Stokes Equations," AIAA 85-0165.

Gnos, A. V., Watson, E. C., Seebaugh, W. R., Sanator, R. J. and DeCarlo, J. P., 1973, "Investigation of Flow Fields Within Large-Scale Hypersonic Inlet Models," NASA TN D-7150.

Ng, W.F., Benson, T. J., and Kunik, W. G., 1986, "Real Gas Effect on the Numerical Simulation of a Hypersonic Inlet," Journal of Propulsion and Power, Vol. 2, No. 4, pp. 381-382.

Ng, W. F.; Ajmari, K,; and Taylor, A. C, III, 1988, "Turbulence Modeling in Hypersonic Flows," AIAA 88-2957.

Ota, D. K., Chakravarthy, S. R., and Darling, J. C., 1988, "An Equilibrium Air Navier-Stokes Code for Hypersonic Flows," AIAA 88-0419.

Rai, M. M., 1985, "A Relaxation Approach to Patched-Grid Calculations with the Euler Equations," AIAA 85-0295.

Roe, P. L., 1981, "Approximate Riemann Solvers, Parameter Vectors, and Difference Schemes," Journal of Computational Physics, Vol. 43, pp. 357-372.

Rudy, D.H., Kumar, A., Thomas, J. L., Gnoffo, P. A. and Chakravarthy, S. R., 1988, "A Comparitive Study and Validation of Upwind and Central-Difference Navier-Stokes Codes for High-Speed Flows," AGARD Symposium on Validation of Computational Fluid Dynamics, Lisbon, Portugal.

Thomas, J. L., van Leer, B., and Walters, R. W., 1985, "Implicit Flux-Split Schemes for the Euler Equations," AIAA 85-1680.

Van Leer, B.; Thomas, J. L.; Roe, P. L.; and Newsome, R. W., 1987," A Comparison of Numerical Flux Formulas for the Euler and Navier- Stokes Equations," AIAA 87-1104CP.

Vatsa, V. N., Thomas, J. L., and Wedan, B. W., 1987, "Navier-Stokes Computations of Prolate Spheroids at Angle of Attack," AIAA 87-2627CP.

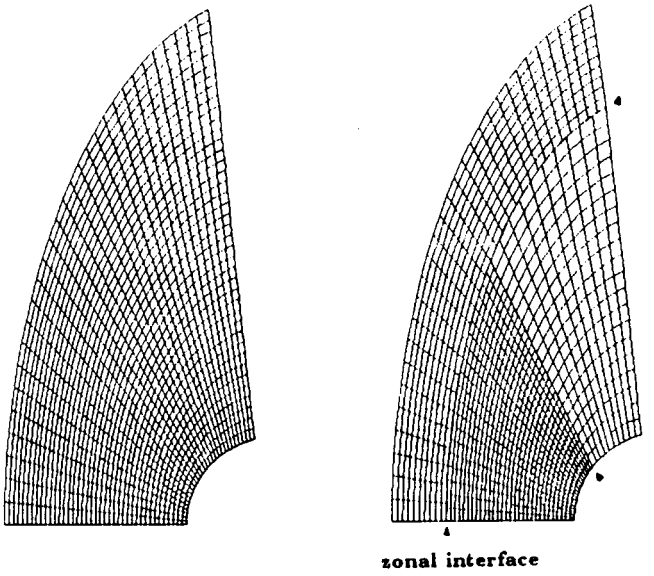

Figure 1. Single and 3-zone grids for blunt body solutions.

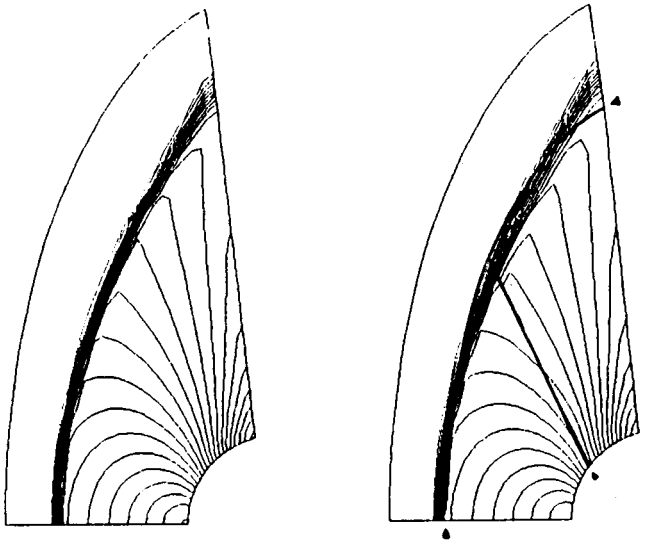

Figure 2. Pressure contours for single and 3-zone grids for blunt body solutions; $M_\infty = 2.0$.

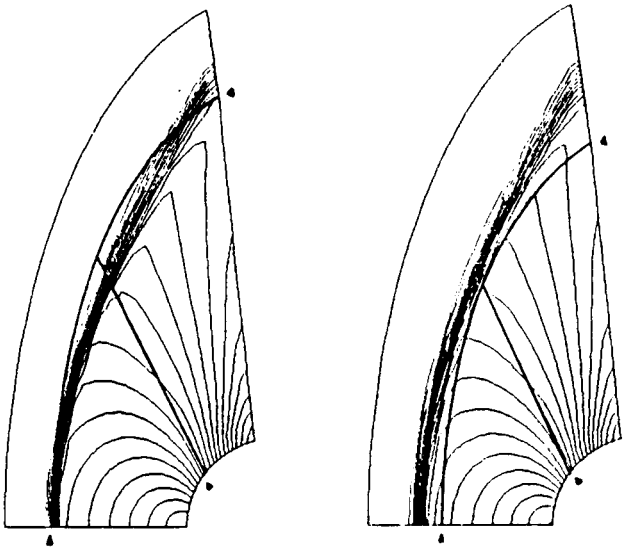

Figure 3. Effect of variations in zonal boundary locations for 3-zone blunt body solutions; $M_\infty = 2.0$

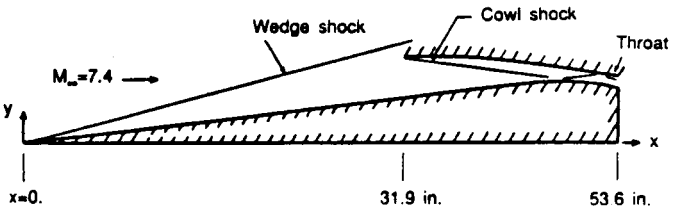

(a.) Sketch of hypersonic inlet configuration for P8 inlet.

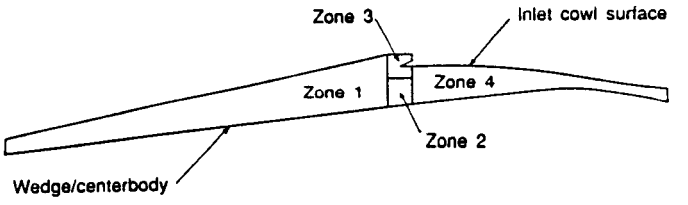

(b.) Zonal topology (P8 inlet).

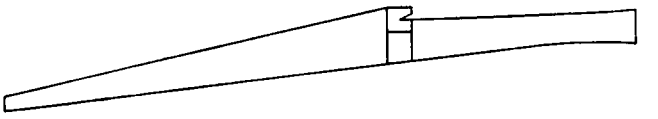

(c.) Zonal topology (P2 inlet).

Figure 4. - Hypersonic inlet configuration and zonal topologies for patched grid computations.

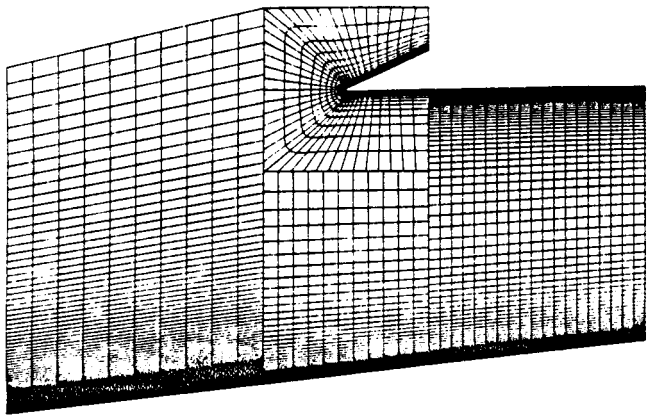

Figure 5. Computational grids near inlet entrance.

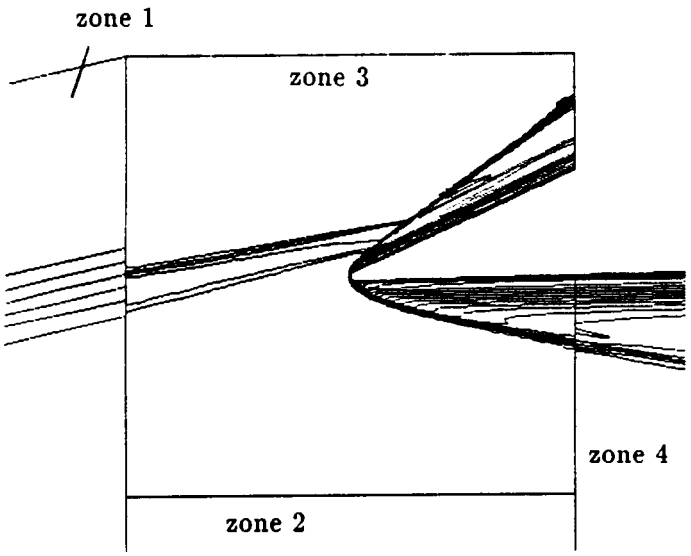

Figure 6. Mach number contours in region of inlet entrance computed with CFL3D Navier-Stokes code.

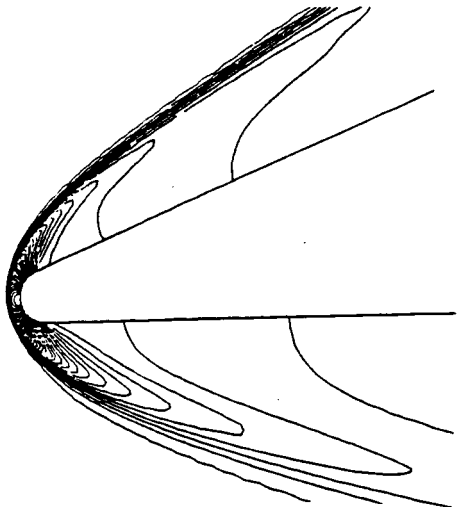

Figure 7. Pressure contours in the region of the blunt cowl lip at inlet entrance station computed with USA-PG2 Navier-Stokes code.

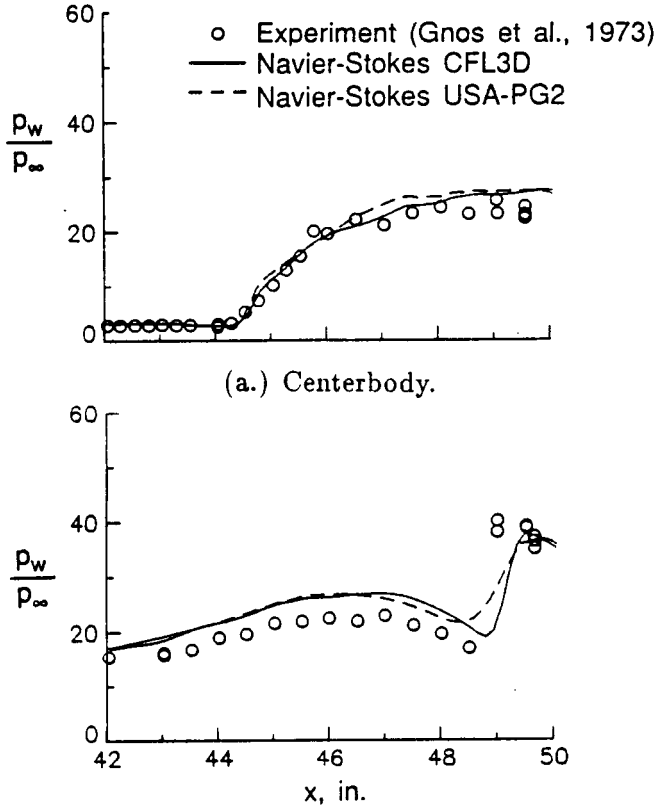

Figure 8. Computed and measured pressures for P8 inlet.

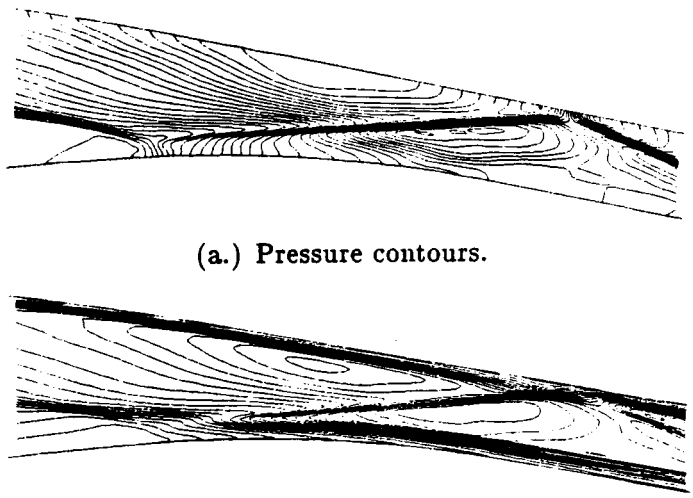

Figure 9. Flowfield contours for P8 inlet computed with CFL3D Navier-Stokes code from x=43 in. to x=50.3 in.

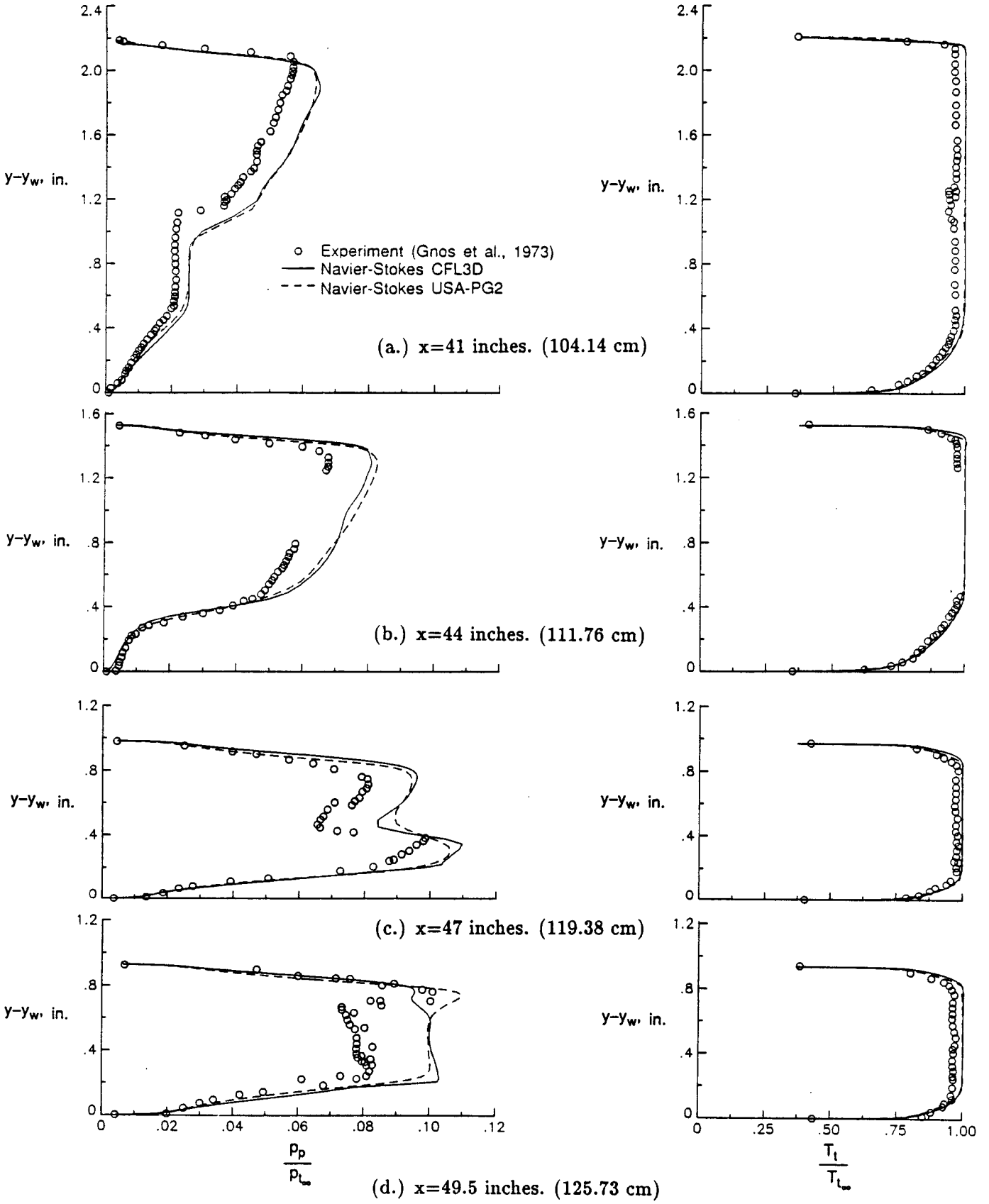

Figure 10. Computed and measured pitot and total temperature profiles for P8 inlet.

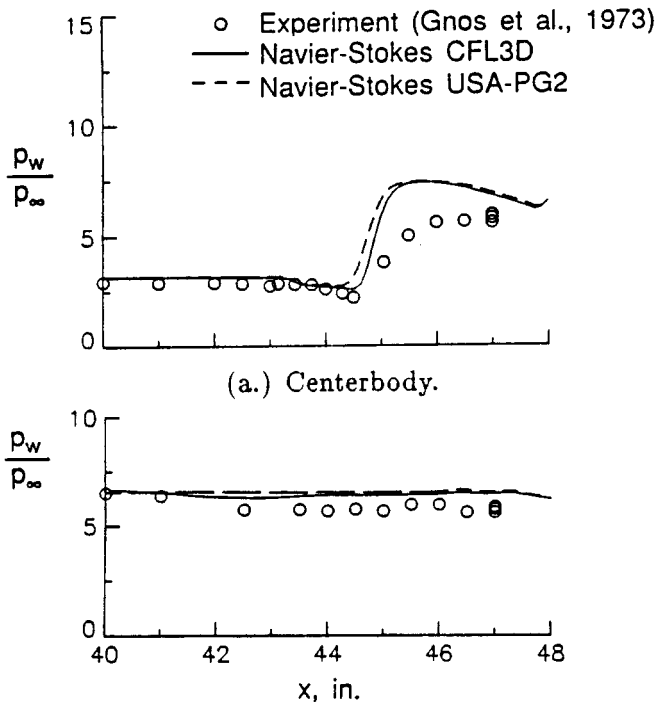

(a.) Centerbody.

(b.) Cowl.

Figure 11. Computed and measured pressures for P2 inlet.

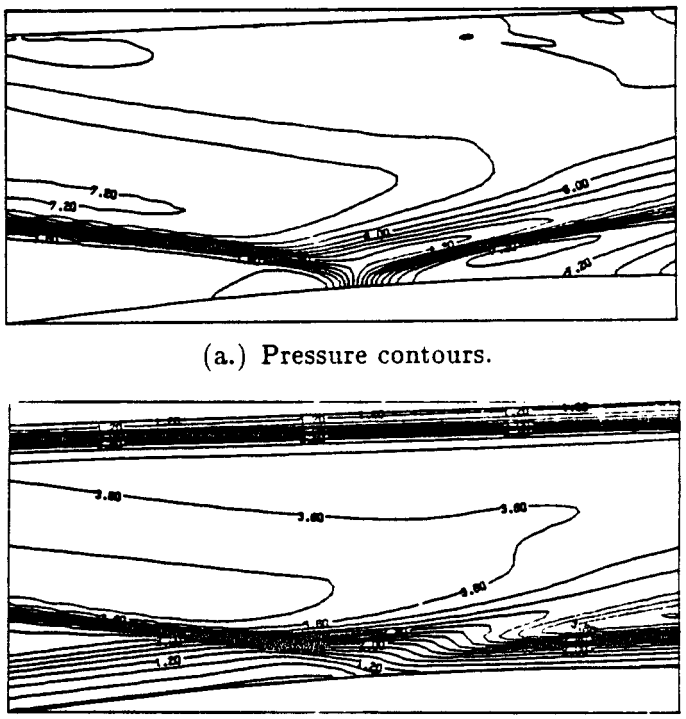

(a.) Pressure contours.

(b.) Density contours.

Figure 12. Flowfield contours for P2 inlet computed with USA-PG2 Navier-Stokes code from x=41.6 in. to x=47.6 in.

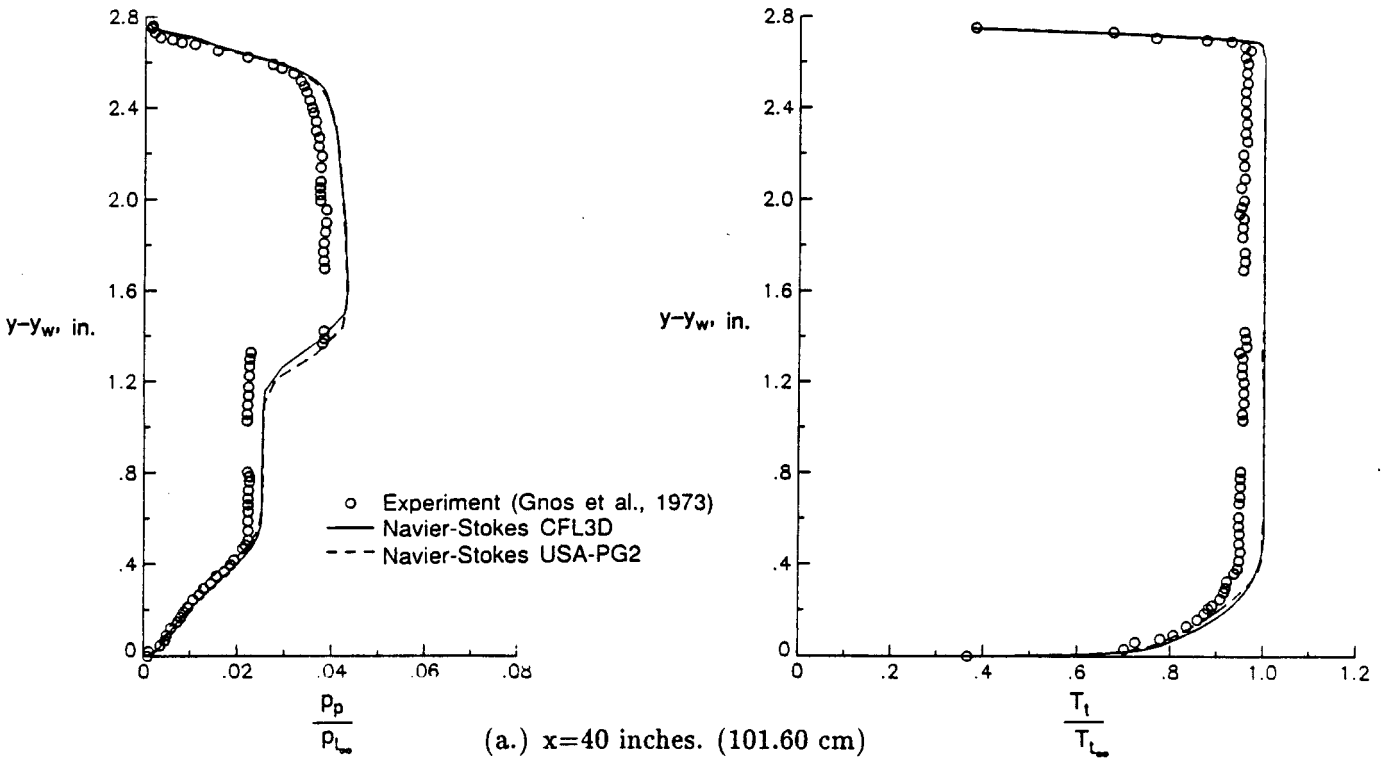

(a.) x=40 inches. (101.60 cm)

Figure 13. Computed and measured pitot and total temperature profiles for P2 inlet.

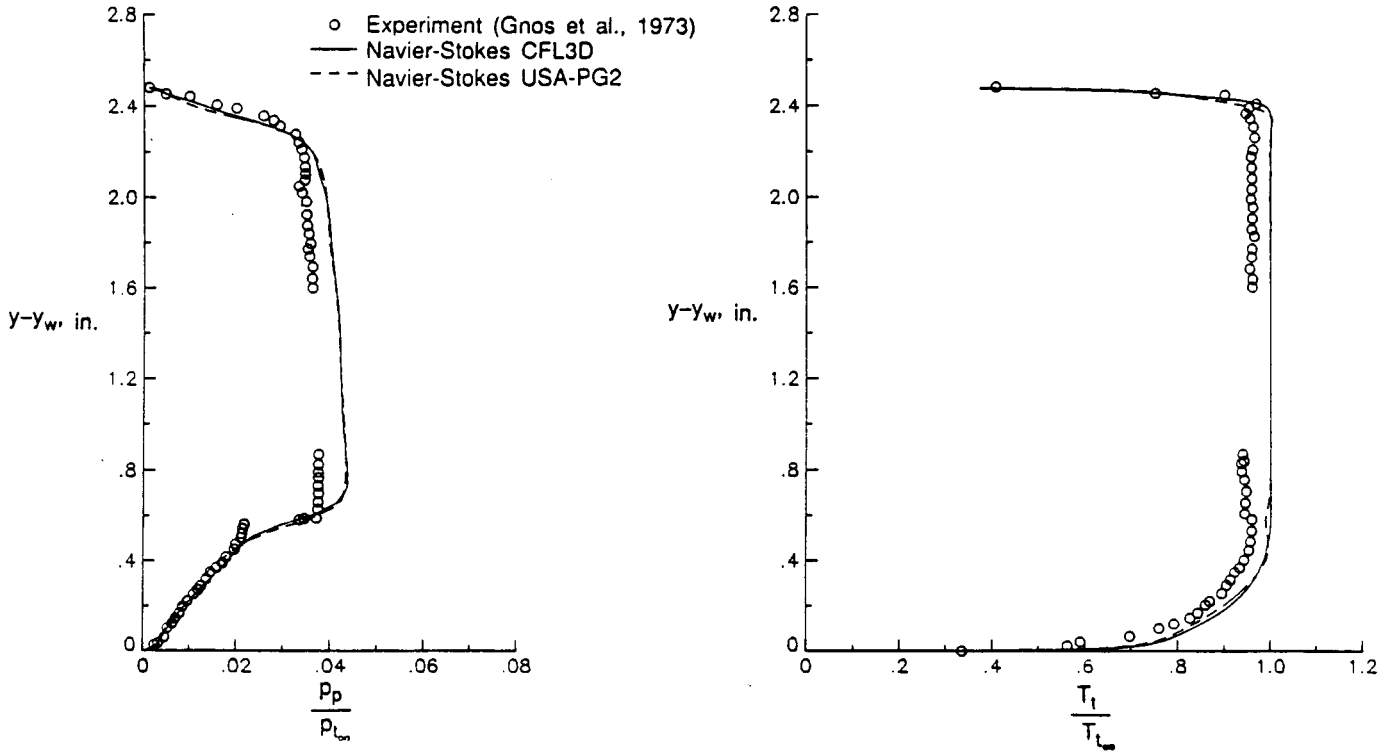

(b.) x=43 inches. (109.22 cm)

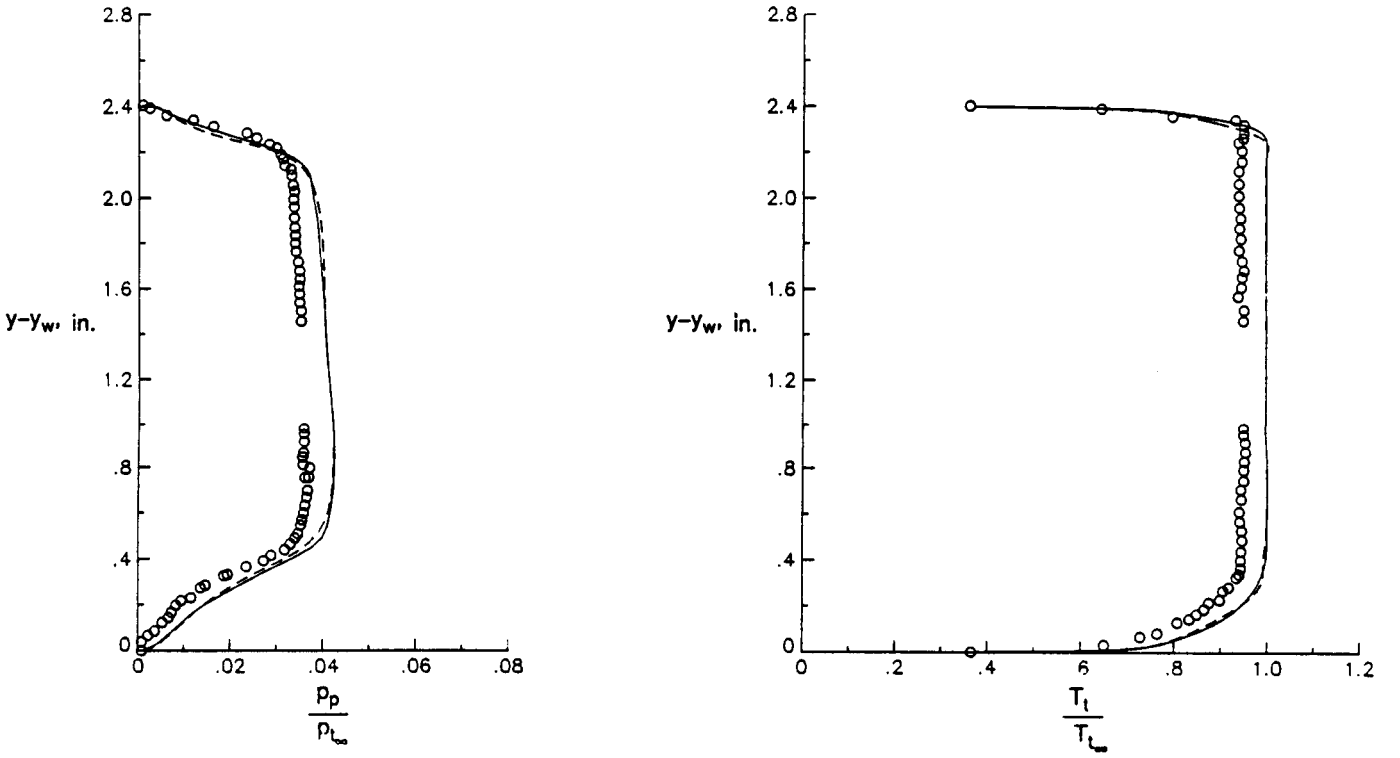

(c.) x=45 inches. (114.30 cm)

Figure 13. Continued.

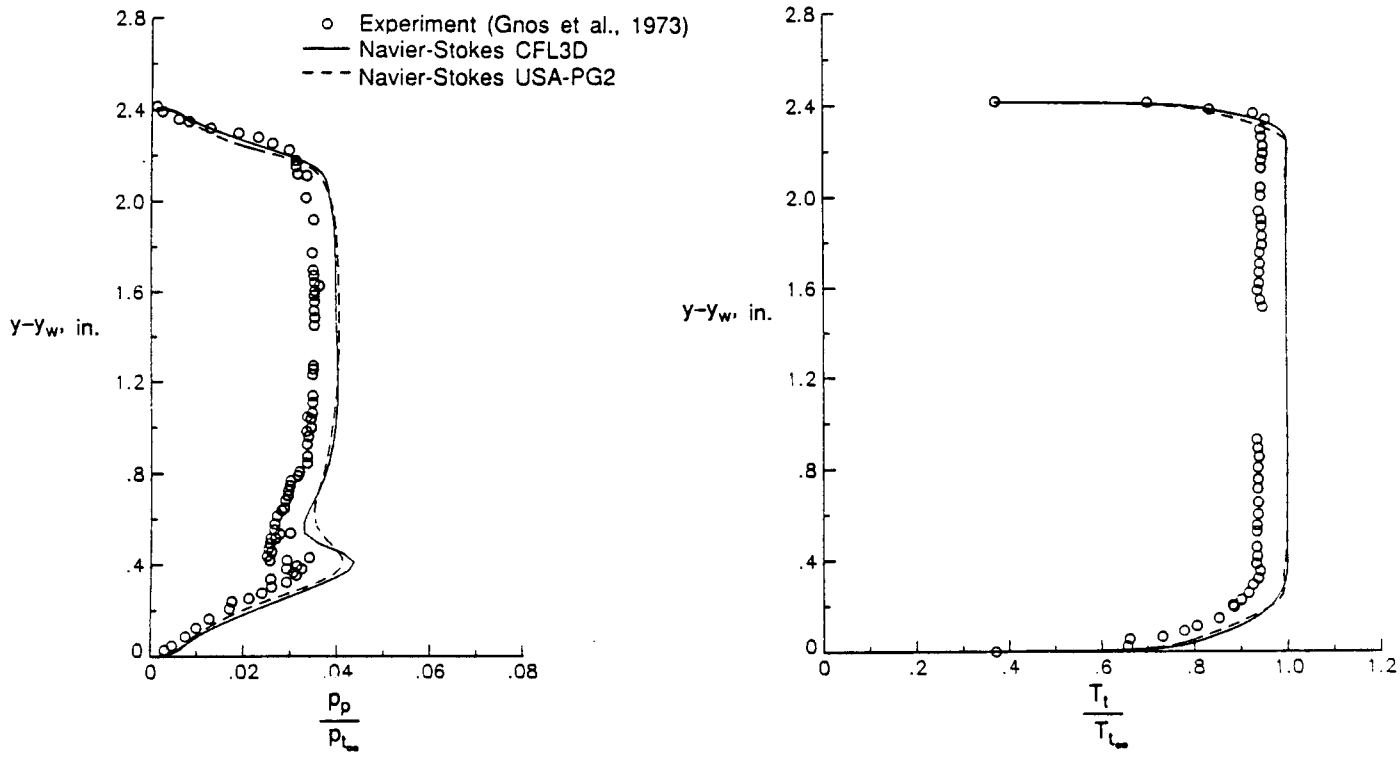

(d.) x=47 inches. (119.38 cm)

Figure 13. Concluded.